

Non-local modulation of the energy cascade in broad-band forced turbulence

Arkadiusz K. Kuczaj* and Bernard J. Geurts†

*Multiscale Modeling and Simulation, J.M. Burgers Center for Fluid Dynamics,
NACM, Department of Applied Mathematics, University of Twente,
P.O. Box 217, 7500 AE Enschede, the Netherlands*

W. David McComb

*School of Physics, University of Edinburgh,
James Clerk Maxwell Building, Mayfield Road,
Edinburgh EH9 3JZ, United Kingdom*

(Dated: October 13, 2018)

Classically, large-scale forced turbulence is characterized by a transfer of energy from large to small scales via nonlinear interactions. We have investigated the changes in this energy transfer process in *broad-band* forced turbulence where an additional perturbation of flow at smaller scales is introduced. The modulation of the energy dynamics via the introduction of forcing at smaller scales occurs not only in the forced region but also in a broad range of length-scales outside the forced bands due to non-local triad interactions. Broad-band forcing changes the energy distribution and energy transfer function in a characteristic manner leading to a significant modulation of the turbulence. We studied the changes in this transfer of energy when changing the strength and location of the small-scale forcing support. The energy content in the larger scales was observed to decrease, while the energy transport power for scales in between the large and small scale forcing regions was enhanced. This was investigated further in terms of the detailed transfer function between the triad contributions and observing the long-time statistics of the flow. The energy is transferred toward smaller scales not only by wavenumbers of similar size as in the case of large-scale forced turbulence, but by a much wider extent of scales that can be externally controlled.

PACS numbers: 47.27.E-, 47.27.Gs, 47.27.Rc

I. INTRODUCTION

The dynamics of kinetic energy plays a central role in turbulent flows. The nonlinear term in the Navier–Stokes equations is responsible for the transfer of energy between any three wavevectors that form a triad in spectral space [1]. Along with the viscous and forcing terms this controls the production, transfer and dissipation of energy in the system. The triadic interactions have been studied for decaying and forced turbulence by many authors (for a review see [2]). Throughout the years various types of large-scale forcing methods [3, 4, 5, 6, 7, 8, 9, 10, 11] have been proposed to sustain quasi-stationarity in numerical turbulence as an idealized form of turbulent flow. The aim of such numerical experiments was to investigate the basic concept of the Kolmogorov (K41) theory [12] that proposes an inertial range in the kinetic energy spectrum and local transfer of energy within this range. The turbulent kinetic energy is on average transferred locally from larger to neighboring smaller scales.

The purpose of this paper is to numerically investi-

gate the processes associated with the flow of energy in a turbulent flow. Specifically, we consider *modulated* turbulence in which the modifications involve the supplementary forcing in a wide range of modes located in an inertial range of the flow. In the literature, mainly turbulence with forcing restricted to the large scales has been examined in detail [2]. The small scale behavior was found to be energetically quite insensitive to the type of forcing and at sufficiently high Reynolds numbers a well-developed inertial range was observed [13]. Against this background, we extend the use of forcing methods and investigate their application directly in the inertial range, thereby focusing particularly on the competition between transfer and forcing. We quantify the dominant alterations due to the broad-band forcing in terms of changes in the energy cascading processes. We pay attention to the energy transfer function and consider changes that arise in the contributions from ‘local’, ‘non-local’ and ‘distant’ triadic interactions. Compared to traditional large-scale forced turbulence, we observe a strengthening of the contributions of non-local interactions, leading to a modification of the inertial range spectrum.

High-resolution direct numerical simulations of turbulence that measure the influence of individual terms in the Navier–Stokes equations on the triadic interactions have been reported [14, 15, 16, 17, 18, 19, 20]. It was found that the energetically dominant triadic interactions involve sets of three modes in which the magnitude of the wavevector of one of the modes differs

*Electronic address: a.k.kuczaj@utwente.nl

†Also: *Anisotropic Turbulence, Fluid Dynamics Laboratory, Department of Applied Physics, P.O. Box 513, 5300 MB Eindhoven, the Netherlands*

considerably from the other two. This suggests that statistics of smaller scales may be affected by larger scales. These dominant processes are not in contradiction with the Kolmogorov theory because the energy is mainly exchanged between the two modes of quite similar wavevector-size [19]. Only a small net energy transfer toward larger wavenumbers arises that involves a detailed cancellation between many individual triad transfers [20]. The spectral space dynamics is characterized by a multitude of separate transfer-processes among various modes. These contributions can be collected in pairs with opposite sign and almost the same magnitude. In total, this leads to a large number of ‘near-cancellations’ and hence only a comparably small net effect remains that constitutes the well-known ‘downward cascading’ toward higher wavenumbers in spectral space. This was confirmed with the use of helical mode decomposition in [20].

The dynamics of actual turbulent flows seen in nature is usually characterized by an enormous number of interacting scales, often perturbed by geometrically complex boundaries and influenced by additional forces such as rotation and buoyancy. This can lead to inhomogeneity and anisotropy, which are not covered directly in the classical view of the Kolmogorov energy cascade and may express themselves in non-local interactions of various particular scales of motion. The complexity of such systems motivated us to study in more detail forcing methods that simultaneously perturb a prescribed range of scales [21]. Such ‘broad-band’ agitation of various scales of motion is observed experimentally in turbulent drag reduction by fibre suspension [22, 23], flows through porous media [24] and over tree canopies [25]. In these cases the energy is transferred abruptly to small scales when the flow reaches an obstruction. Various other types of flows also exhibit turbulent motions that coexist at different scales [26].

To explore the possibilities of a broader application of forcing methods in turbulence modeling and concurrently examine the energy dynamics in flows that do not directly follow the classical Kolmogorov $-5/3$ scaling we employ numerical simulations of *broad-band* forced turbulence. The forcing studied in this paper represents a continual addition/removal of energy from a broad range of scales in the system, thereby providing the possibility of altering the characteristic $-5/3$ slope in the kinetic energy spectrum as predicted by the K41 theory. Specifically, as indicated in Fig. 1, we apply the forcing to two regions. The large-scale forcing $k \leq k_0$ classically agitates the largest scales in a flow while the additional band $k_1 < k \leq k_2$ is located in a region of the inertial regime, to allow a direct competition with the nonlinear transfer term. For inertial-range scales broad-band forcing introduces explicit energy injection next to the transfer-term. We varied the spectral support and strength of the high- k band to investigate the modulation of the turbulence that develops. This distinguishes it from the classical forcing of large scales only.

In this paper we compute changes in the energy distribution associated with the broad-band forcing and ob-

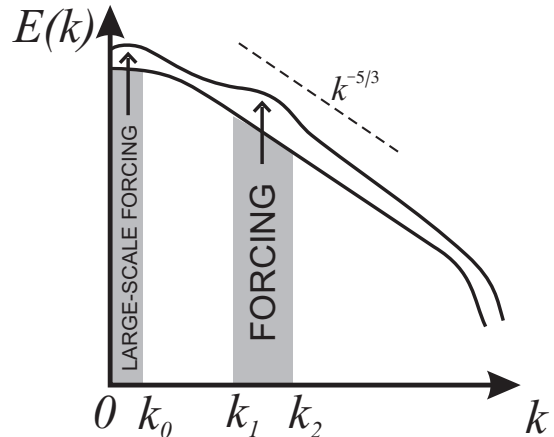


FIG. 1: Broad-band forcing in spectral space. Large-scale forcing $k \leq k_0$ with an additional high- k forced region $k_1 < k \leq k_2$.

serve a characteristic alteration in the spectral energy transfer compared to the classical Kolmogorov cascading. This alteration expresses itself by additional local minima and maxima in the transfer function. It is well known that in cases with large-scale forcing only, negative values are found for the transfer at the smallest wavenumbers indicating the energy injection at these scales. The positive values for the transfer that arise for all other wavenumbers indicates the energy cascading process to smaller scales. In our case of broad-band forcing in the inertial range, additional negative regions appear in the transfer function. These coincide with the additional local injection of energy. Such a negative region is bordered by nearby additional maxima in the transfer. These characterize the associated increased energy transfer to scales just larger or just smaller than the broad-band forced region.

Forcing applied to different spatial scales simultaneously allows a non-local modulation of the energy distribution compared to the reference Kolmogorov case. To quantify the alterations in the energy transfer we use a decomposition of the velocity field closely following [16] and investigate the magnitude of the contributions from various spatial scales to the overall energy transfer.

The main finding of this study pertains to the role of broad-band inertial range forcing in modifying the natural energy cascading process. This is understood explicitly in terms of changes in the detailed non-local energy transfer. In addition, we illustrate and quantify the mechanism of enhancement of the total energy transfer to smaller scales arising from broad-band forcing and the depletion of the energy-content in the large scales. Agitation of certain high wavenumbers can affect well separated low wavenumber components in a flow. These findings may be relevant for problems that involve the control of turbulent flow in complex geometries in which various scales of motions are simultaneously agitated, e.g.,

in compact heat-exchangers [24]. Further applications of such broad-band forcing may be connected with the observed modulations of transport properties in physical space leading to an enhanced scalar dispersion rate [21].

The organization of this paper is as follows. The mathematical formulation of the problem is given in Sec. II where the computational method and the energy transfer terms are also described. The energy spectra of broad-band forced turbulence and the modulation of the energy transfer are investigated in Sec. III. In Sec. IV we present a more detailed view of the energy transfer processes by computing partitioned energy transfer function over various spatial scales. The paper closes with a summary in Sec. V.

II. COMPUTATIONAL FLOW MODEL

An overview of the computational model is given in this section (II A). The forcing method in the broad-band context is described subsequently (II B). In addition, the energy transfer between different triads is partitioned in a number of contributions (II C) that will be studied numerically in Sec. IV. Finally, simulation details are given (II D).

A. Equations of motion

The incompressible Navier–Stokes equations in spectral (Fourier) representation can be written as

$$(\partial_t + \nu k^2) u_\alpha(\mathbf{k}, t) = \Psi_\alpha(\mathbf{k}, t) + F_\alpha(\mathbf{k}, t), \quad (1)$$

where $u_\alpha(\mathbf{k}, t)$ is the velocity field coefficient at wavevector \mathbf{k} ($k = |\mathbf{k}|$) and time t [1]. The non-dimensional kinematic viscosity ν is the inverse of the computational Reynolds number ($Re = 1/\nu$). The nonlinear term reads

$$\Psi_\alpha(\mathbf{k}, t) = M_{\alpha\beta\gamma} \sum_{\mathbf{p}+\mathbf{q}=\mathbf{k}} u_\beta(\mathbf{p}, t) u_\gamma(\mathbf{q}, t), \quad (2)$$

and the forcing term $F_\alpha(\mathbf{k}, t)$ is specified in section II B. The tensor $M_{\alpha\beta\gamma}$ in (2) accounts for the pressure and incompressibility effects:

$$M_{\alpha\beta\gamma} = \frac{1}{2i} (k_\beta D_{\alpha\gamma} + k_\gamma D_{\alpha\beta}), \quad (3)$$

in which

$$D_{\alpha\beta} = \delta_{\alpha\beta} - k_\alpha k_\beta / k^2. \quad (4)$$

Taking the inner product of (1) and $u_\alpha^*(\mathbf{k}, t)$, where the asterisk denotes the complex conjugate, we obtain the energy equation

$$(\partial_t + 2\nu k^2) E(\mathbf{k}, t) = T(\mathbf{k}, t) + T_F(\mathbf{k}, t). \quad (5)$$

The spectral energy density is denoted by $E(\mathbf{k}, t) = \frac{1}{2} u_\alpha^*(\mathbf{k}, t) u_\alpha(\mathbf{k}, t)$. The rate of energy exchanged at wavevector \mathbf{k} with all other modes in the system is characterized by the energy transfer function

$$T(\mathbf{k}, t) = u_\alpha^*(\mathbf{k}, t) \Psi_\alpha(\mathbf{k}, t). \quad (6)$$

The rate of energy provided by the forcing term is

$$T_F(\mathbf{k}, t) = u_\alpha^*(\mathbf{k}, t) F_\alpha(\mathbf{k}, t), \quad (7)$$

and the energy dissipation rate present in (5) reads

$$\varepsilon(\mathbf{k}, t) = 2\nu k^2 E(\mathbf{k}, t). \quad (8)$$

The three terms $T(\mathbf{k}, t)$, $T_F(\mathbf{k}, t)$ and $\varepsilon(\mathbf{k}, t)$ represent the energy dynamics in the system that each typically act in distinct wavenumber regions. The forcing term $T_F(\mathbf{k}, t)$ is non-zero in the forced modes only. In this paper the collection of forced modes will always contain a low wavenumber band corresponding to large-scale forcing of the flow. In addition, higher wavenumber contributions will be included in $T_F(\mathbf{k}, t)$. In contrast, the energy dissipation rate $\varepsilon(\mathbf{k}, t)$ is defined in the entire spectral space, but it is dynamically important primarily for the high wavenumber range. Finally, the transfer term $T(\mathbf{k}, t)$ is basic to the development of an energy cascade and is a dominant contribution for wavenumbers in an inertial range [1].

The change of the total energy \widehat{E} in the system is connected with its viscous dissipation and the total effect of the forcing. In fact, introducing

$$\widehat{E}(t) = \sum_{\mathbf{k}} E(\mathbf{k}, t), \quad (9)$$

we find

$$\partial_t \widehat{E}(t) = \widehat{T}_F(t) - \widehat{\varepsilon}(t), \quad (10)$$

where $\widehat{\varepsilon}(t) = \sum_{\mathbf{k}} \varepsilon(\mathbf{k}, t)$ and $\widehat{T}_F(t) = \sum_{\mathbf{k}} T_F(\mathbf{k}, t)$. We used the fact that the total energy transfer $\widehat{T}(t) = \sum_{\mathbf{k}} T(\mathbf{k}, t) = 0$. The injection of energy occurs only in the forced region. This keeps the whole system in a quasi-stationary state. Normally, the forced region is restricted to the largest scales in a flow represented by the smallest wavenumbers [5, 10]. The energy introduced in the large scales is transferred to smaller scales and dissipated primarily in very localized flow-features of viscous length-scales. By the introduction of an additional source of energy in the inertial range we will study the perturbation of the energy cascading process by the forcing. The forcing method adopted here will be presented next.

B. Forcing method

Forcing is achieved by applying an additional driving $F_\alpha(\mathbf{k}, t)$ to the velocity field in Fourier space, cf. (1).

Conventionally, the turbulent cascade develops as a statistical equilibrium is reached, characterized by the balance between the input of kinetic energy through the forcing and its removal through viscous dissipation. In literature ([3, 4, 5, 6, 7, 8, 9, 10, 11]), we may distinguish several numerical approaches to forced turbulence that all refer to the agitation of the largest scales of motion. Here, we modify such classical forcing procedures by allowing for the simultaneous agitation of a broader range of intermediate- k modes as depicted in Fig. 1.

We study two ranges of forcing: the classical large-scale forcing ($k \leq k_0$) and small-scale forcing localized in the spectral region where the transfer of energy $T(\mathbf{k}, t)$ is important ($k_1 < k \leq k_2$). By narrowing or widening the width of the forced bands, along with a change in their location in spectral space we can control several aspects of the energy-dynamics. The strength of forcing is controlled by the amount of energy introduced to various regions in spectral space.

We expect the small-scale forcing band to influence the inter-scale energy transfer process not only between scales of similar size but at a wider spectrum of scales. This may be understood globally as follows. The process of energy cascading is mainly interpreted via the resulting local transfer of energy in spectral space [19]. However, this total energy transfer results from many non-local contributions and these may be directly altered by the additional small-scale forcing. Correspondingly an influence on the overall energy cascading process may occur over an extended wavenumber range. We quantify this effect by evaluating the nonlinear interactions among the various modes while they are being perturbed by the broad-band forcing.

In this paper we adopt the recently proposed fractal forcing [27], which involves a power-law dependence of F_α on the wavenumber:

$$F_\alpha(\mathbf{k}, t) = \tilde{\varepsilon}_w(\mathbf{k}) \frac{k^\beta e_\alpha(\mathbf{k}, t)}{\sum_{\mathbf{k} \in \mathbb{K}} k^\beta \sqrt{2E(\mathbf{k}, t)}}, \quad (11)$$

where the coefficient $\beta = D_f - 2$ is connected with the fractal dimension D_f of the stirrer and $\tilde{\varepsilon}_w(\mathbf{k})$ is the energy input rate at mode \mathbf{k} . The set of forced modes \mathbb{K} is composed of bands $\mathbb{K}_{m,p}$ ($m \leq p$) which consist of $p - m + 1$ adjacent spherical shells $\mathbb{S}_n = \frac{2\pi}{L_b}(n - 1/2) < |\mathbf{k}| \leq \frac{2\pi}{L_b}(n + 1/2)$: $m \leq n \leq p$, in terms of the size of the computational domain denoted by L_b . In the simulations we always force the first shell \mathbb{S}_1 and a single high- k band $\mathbb{K}_{m,p}$, if not stated otherwise. The classical large-scale forcing of the first shell \mathbb{S}_1 has a constant energy injection rate $\varepsilon_{w,1}$ in (11) while $\mathbb{K}_{m,p}$ has a constant strength $\varepsilon_{w,2}$ and a support in spectral space controlled by m and p :

$$\tilde{\varepsilon}_w(\mathbf{k}) = \begin{cases} \varepsilon_{w,1} & \text{if } \mathbf{k} \in \mathbb{S}_1, \\ \varepsilon_{w,2} & \text{if } \mathbf{k} \in \mathbb{K}_{m,p}, \\ 0 & \text{otherwise.} \end{cases} \quad (12)$$

The vector \mathbf{e} in (11) is given by [27]:

$$\mathbf{e}(\mathbf{k}, t) = \frac{\mathbf{u}(\mathbf{k}, t)}{|\mathbf{u}(\mathbf{k}, t)|} + i \frac{\mathbf{k} \times \mathbf{u}(\mathbf{k}, t)}{|\mathbf{k}| |\mathbf{u}(\mathbf{k}, t)|}. \quad (13)$$

This vector consists of two parts, either parallel or perpendicular to the vector $\mathbf{u}(\mathbf{k}, t)$. In this forcing procedure, we have control over the energy input rate, the range of forced modes and the effective geometrical complexity of the stirrer represented by the fractal dimension.

The summation over all forced modes of $u_\alpha^*(\mathbf{k}, t) F_\alpha(\mathbf{k}, t)$ yields a total energy input rate given by:

$$\widehat{T}_F(t) = \sum_{\mathbf{k}} T_F(\mathbf{k}, t) = \sum_{\mathbf{k}} u_\alpha^*(\mathbf{k}, t) F_\alpha(\mathbf{k}, t) = \varepsilon_w, \quad (14)$$

where $\varepsilon_w = \varepsilon_{w,1} + \varepsilon_{w,2}$. The energy input leads to a quasi-stationary state described by the energy equation

$$\partial_t \widehat{E}(t) = \varepsilon_w - \widehat{\varepsilon}(t). \quad (15)$$

This characterizes the energy dynamics in the system at the most global level. We observe that this forcing implies a constant energy injection rate that results in a fluctuating total energy \widehat{E} and a fluctuating total energy dissipation rate with mean ε_w .

In the next subsection a more detailed description of the energy dynamics will be given based on the processes that are responsible for its transfer.

C. Energy transfer

A detailed investigation of the energy transfer in large-scale forced turbulence [19] shows that the dominant triadic interactions occur between wavevectors of quite different lengths. Hence, large-scale forcing may be directly involved in the dynamics of much smaller scales [28]. The interactions are roughly classified as ‘‘local’’ when the sizes of all wavevectors in a triad are similar, ‘‘non-local’’ when the scale separation is about a factor 10-15 and ‘‘distant’’ when the separation is much larger [29]. It was shown that the transfer of energy reaches maximum values for triads with two wavevectors of similar size and one with quite different length [19]. Although, the interactions between triads can be seen mainly as non-local, the dominant net energy transfer is local, i.e., occurring between similar scales [13, 30, 31]. The interactions produce forward and backward energy transfer that combined result in a small net forward energy transfer because of the detailed balance between contributions that virtually cancel each other [20]. The forward cascade in the inertial range was found to be dominated by local and non-local interactions, while the distant interactions do not significantly transfer energy [29]. All these findings concern the classical turbulence forced at the largest scales.

Against this background, we ask what the turbulence response will be to a broad-band perturbation of the energy transfer processes? In recent literature a somewhat

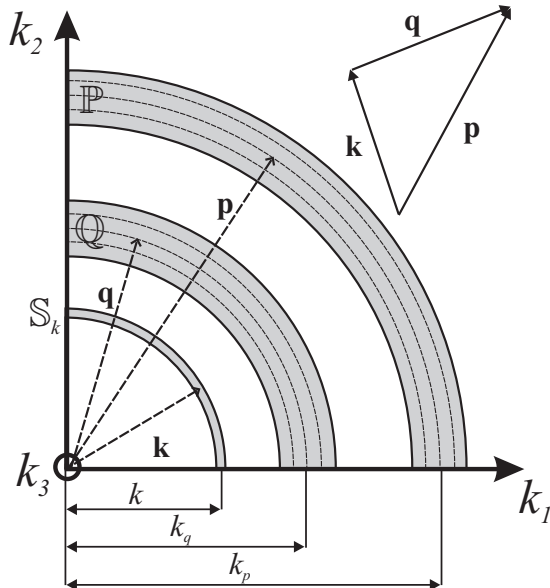


FIG. 2: Schematic triadic interaction that occurs between wavevector \mathbf{k} in shell \mathbb{S}_k and wavenumbers \mathbf{p} , \mathbf{q} taken from regions \mathbb{P} and \mathbb{Q} of spectral space that each consist of four shells with central wavenumbers k_p and k_q .

related study was reported in [32]. Decaying turbulence that starts from an initial condition with an energetically strongly enhanced small-scale band of modes was studied. The presence of the extra small-scale band was found to reduce the intensity of the developing turbulence by enhancing the *non-local energy cascade* directly towards smaller scales. This removes the kinetic energy more efficiently. The energy feeding mechanisms and energy transfer also attract much attention in transitional and turbulent flows with an active control [33]. The modulation induced by the broad-band forcing has its consequences not only in the spectral space dynamics of a flow but also in its physical space transport properties [21].

To analyze the response of turbulence to the additional broad-band perturbation in more detail we apply previously developed methods used in the examination of energy transfer in large-scale forced turbulence [16]. Referring to Fig. 2, the energy transfer between a wavevector $\mathbf{k} = (k_1, k_2, k_3)$ and all pairs of wavevectors \mathbf{p} and $\mathbf{q} = \mathbf{k} - \mathbf{p}$ with \mathbf{p} , \mathbf{q} chosen in some prescribed regions \mathbb{P} and \mathbb{Q} will be investigated. Such a decomposition allows measuring the contribution of separate scales to the transfer function $T(\mathbf{k}, t)$. The precise specification requires a few steps that are presented next. First, we define the truncated velocity field as

$$u_{\alpha}^{(\mathbb{P}, \mathbb{Q})}(\mathbf{k}, t) = \begin{cases} u_{\alpha}(\mathbf{k}, t) & \text{if } \mathbf{k} \in \mathbb{P} \text{ or } \mathbf{k} \in \mathbb{Q}, \\ 0 & \text{otherwise.} \end{cases} \quad (16)$$

Based on this truncated velocity field we may compute the energy transfer involving the wavevector \mathbf{k} and all

wavevectors \mathbf{p} and \mathbf{q} :

$$T_{\mathbb{P}\mathbb{Q}}(\mathbf{k}, t) = \begin{cases} \tilde{T}_{\mathbb{P}\mathbb{P}}(\mathbf{k}, t) & \text{if } \mathbb{P} = \mathbb{Q}, \\ \frac{1}{2}(\tilde{T}_{\mathbb{P}\mathbb{Q}}(\mathbf{k}, t) - \tilde{T}_{\mathbb{P}\mathbb{P}}(\mathbf{k}, t)) & \\ -\tilde{T}_{\mathbb{Q}\mathbb{Q}}(\mathbf{k}, t) & \text{if } \mathbb{P} \neq \mathbb{Q}, \end{cases} \quad (17)$$

where

$$\tilde{T}_{\mathbb{P}\mathbb{Q}}(\mathbf{k}, t) = u_{\alpha}^*(\mathbf{k}, t) \Psi_{\alpha}^{(\mathbb{P}, \mathbb{Q})}(\mathbf{k}, t). \quad (18)$$

The nonlinear term $\Psi_{\alpha}^{(\mathbb{P}, \mathbb{Q})}(\mathbf{k}, t)$ is defined by the convolution of the truncated fields:

$$\Psi_{\alpha}^{(\mathbb{P}, \mathbb{Q})}(\mathbf{k}, t) = M_{\alpha\beta\gamma} \sum_{\mathbf{p}+\mathbf{q}=\mathbf{k}} u_{\beta}^{(\mathbb{P}, \mathbb{Q})}(\mathbf{p}, t) u_{\gamma}^{(\mathbb{P}, \mathbb{Q})}(\mathbf{q}, t), \quad (19)$$

where the sum is over all triads with $\mathbf{p} \in \mathbb{P}$ and $\mathbf{q} \in \mathbb{Q}$ such that $\mathbf{p} + \mathbf{q} = \mathbf{k}$.

For a statistically isotropic, homogeneous turbulence it is convenient to average over spherical shells in wavevector space. In addition, in view of the considerable computational effort involved in computing all interactions between the very large number of scales present in the flow, we introduced a slight coarse-graining in terms of the regions \mathbb{P} and \mathbb{Q} as shown in Fig. 2. Specifically, it was found adequate to group together contributions from four adjacent shells. Other more coarse ‘groupings’ of wavenumbers have been considered in the literature with the aim of extracting the dominant interaction processes at a reasonable computational effort. As an example a ‘logarithmic’ grouping was adopted in [16] combining contributions from bands with a width of 2^k . In this paper we will look at the interactions of four shells \mathbb{P} at distance k_p (cf. Fig. 2) with four shells \mathbb{Q} at distance k_q that contribute to the nonlinear energy transfer to shell \mathbb{S}_k characterized by the wavenumber k .

In terms of the transfer function $T_{\mathbb{P}\mathbb{Q}}(\mathbf{k}, t)$ we may now define the required spectral transfer functions. The energy transfer term (17) gives the exchange of energy by the triad $(\mathbf{k}, \mathbf{p}, \mathbf{q})$ where the latter two wavevectors are specified by the sets \mathbb{P} and \mathbb{Q} and the triangle constraint. Summing over all modes \mathbf{k} in shell \mathbb{S}_k we obtain the exact exchange of energy in the k -th shell between k , k_p and k_q :

$$T_{pq}(k, k_p, k_q, t) = \sum_{\mathbf{k} \in \mathbb{S}_k} T_{\mathbb{P}\mathbb{Q}}(\mathbf{k}, t). \quad (20)$$

We refer to T_{pq} as the ‘three-mode’ transfer. The total energy transfer function $T(k, t)$ can be computed directly from (6) or as sum of the contributions from (20):

$$T(k, t) = \sum_{k_p} T_p(k, k_p, t), \quad (21)$$

in which the ‘two-mode’ transfer T_p is given by:

$$T_p(k, k_p, t) = \sum_{k_q} T_{pq}(k, k_p, k_q, t). \quad (22)$$

The individual transfer-terms $T(k, t)$, $T_p(k, k_p, t)$ and $T_{pq}(k, k_p, k_q, t)$ give respectively more detailed characteristics of the energy transfer. The total transfer $T(k, t)$ expresses the amount of energy transferred from (negative) or to (positive) shell \mathbb{S}_k . All three transfer-terms T , T_p and T_{pq} will be used to investigate the transfer of energy in the sequel.

D. Simulation details

The numerical integration of the Navier–Stokes equations (1) is done via a four-stage, second-order, compact-storage, Runge-Kutta method [34]. To fully remove the aliasing error we applied a method that employs two shifted grids and spherical truncation [35]. We consider the canonical problem of forced turbulence in a cubic box of side L_b with periodic boundary conditions. Direct numerical simulations are characterized by N^3 computational points, where N is the number of grid-points used in each direction. A detailed description of the simulation setup and the validation of the numerical procedure can be found in [21]. The components of the wavevector \mathbf{k} are $k_\alpha = (2\pi/L_b)n_\alpha$ where $n_\alpha = 0, \pm 1, \pm 2, \dots, \pm(N/2 - 1), -N/2$ for $\alpha = 1, 2, 3$. The numerical simulations are defined further by the size of the domain ($L_b=1$), the computational Reynolds number Re and the energy injection rates to the two distinct bands ($\varepsilon_{w,1}, \varepsilon_{w,2}$).

We will study this homogeneous turbulent flow at two different computational Reynolds numbers, i.e., $Re = 1061$ and $Re = 4243$. In case of homogeneous, decaying turbulence these Reynolds numbers correspond to $R_\lambda = 50$ or 100 , in terms of the initial Taylor-Reynolds number [21]. The large-scale forcing of \mathbb{S}_1 has an energy injection rate $\varepsilon_{w,1} = 0.15$ that is used as reference case. For all simulations the fractal dimension was kept constant and equal to $D_f = 2.6$ [27]. The smallest length-scale that should be accurately resolved depends on the size of the box, viscous dissipation and energy injection rate. Usually it is required that $k_{\max}\eta > 1$ [5, 36, 37] in terms of the Kolmogorov length-scale η and the maximal magnitude of the wavevector $k_{\max} = \pi N/L_b$ that enters the computations. In our simulations $k_{\max}\eta \gtrsim 2$ indicating that the small scales are well resolved.

We consider time-averaged properties of the turbulent flow. For a function h these are defined by

$$\langle h \rangle_t = \lim_{t \rightarrow \infty} \frac{1}{t - t_0} \int_{t_0}^t h(\tau) d\tau \approx \frac{1}{\mathcal{T} - t_0} \int_{t_0}^{\mathcal{T}} h(\tau) d\tau, \quad (23)$$

where \mathcal{T} is sufficiently large. We start the averaging at $t_0 = 5$ which corresponds to about 10 eddy-turnover times for the simulated cases. The final time was taken equal to $\mathcal{T} = 30$, so all results are averaged over approximately 50 eddy-turnover times. The accuracy of this approximation to the long-time average, measured as the

ratio of the standard deviation and the mean signal is less than 5% for all investigated quantities.

The energy spectra presented in this paper are shell- and time-averaged. Moreover, we focus on compensated spectra E_c in which we use non-dimensional Kolmogorov units: $E_c(k) = \langle \hat{\varepsilon} \rangle_t^{-2/3} k^{5/3} \langle E_s(k, t) \rangle_t$ in terms of the shell-averaged spectrum $E_s(k, t) = \sum_{\mathbf{k} \in \mathbb{S}_k} E(\mathbf{k}, t)$. The compensation of the spectrum is not strictly required to observe the characteristic changes in the energy distribution, but as it gives more information about the dominant scales present in a flow it will be used throughout.

III. BROAD-BAND FORCED TURBULENCE

To investigate the energy dynamics in broad-band forced turbulence, first the influence of variation of the strength and location of the second forced band $\mathbb{K}_{m,p}$ on the global characteristics and spectrum of the flow is presented (III A). Then we examine in more detail the effects of these variations on the energy distribution and transfer characteristics in the system (III B).

A. Energy distribution in forced turbulence

We first concentrate on the application of the high- k forcing band at *different locations* in spectral space. We apply a constant energy input rate $\varepsilon_{w,2} = 0.15$ to this band. Simultaneously, the large-scale forcing to the first shell \mathbb{S}_1 is $\varepsilon_{w,1} = 0.15$. The computational Reynolds number is $Re = 1061$. We forced the bands $\mathbb{K}_{p,p+3}$ for $p = 5, 9, 17, 25$. The parameters of these simulations with some of the statistics are further presented in the Appendix (Runs 1 and 14 – 17 in Table I and II are concerned here).

The total kinetic energy, energy dissipation rate and Taylor-Reynolds number are shown in Fig. 3 as a function of the location of the left-boundary p of the high- k forced band $\mathbb{K}_{p,p+3}$. The first data point refers to the classical large-scale forcing only (Run 1). Application of broad-band forcing in the different bands changes the characteristics of the flow modifying primarily the amount of small scales. This forcing in the second band is seen to increase the energy dissipation in the system. The Kolmogorov dissipation-scale and the Taylor-Reynolds number decrease, suggesting that the characteristic scale at which dissipation plays an important role is shifted to smaller scales. We notice that the total energy in the system is only slightly affected by the introduction of forcing. Moving the broad-band forcing to very small scales implies that there is no longer a strong influence on the flow because the energy injected in the small scales appears to be also dissipated immediately.

The compensated, shell- and time-averaged, energy spectrum for different locations of the forced region $\mathbb{K}_{p,p+3}$ is shown in Fig. 4. We may observe that the

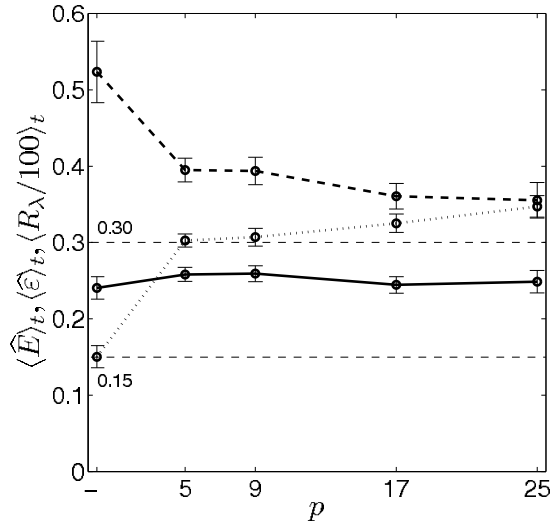


FIG. 3: Time-averaged total kinetic energy \widehat{E} (solid), total energy dissipation rate $\widehat{\varepsilon}$ (dotted) and Taylor-Reynolds number R_λ (dashed) for forced turbulence with different locations of the second band at $Re = 1061$.

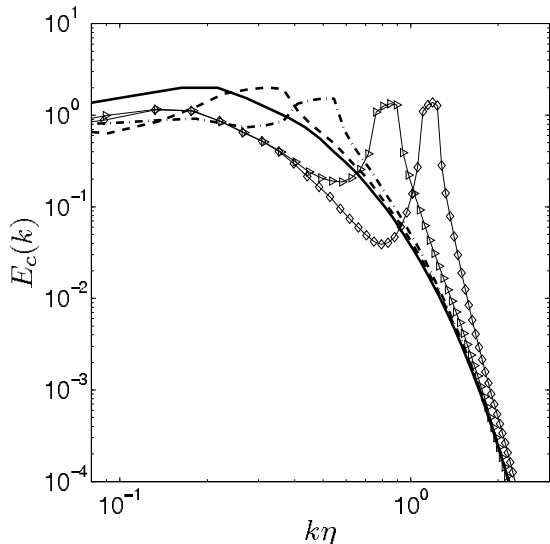


FIG. 4: Compensated shell- and time-averaged energy spectrum $E_c(k)$ for two-band forcing: \mathbb{S}_1 and $\mathbb{K}_{p,p+3}$. Large-scale forcing \mathbb{S}_1 (solid), additional forcing in the second band $\mathbb{K}_{5,8}$ (dashed), $\mathbb{K}_{9,12}$ (dash-dotted), $\mathbb{K}_{17,20}$ (\triangleright), $\mathbb{K}_{25,28}$ (\diamond) at $Re = 1061$.

forcing causes a non-local depletion in the energy spectrum for the larger scales while the tail of the spectrum is less affected. The pile up in the energy spectrum near the forcing region is characteristic of the explicit high- k forcing and is suggestive of a ‘blocking’ or reverse cascading. If the separation between \mathbb{S}_1 and the high- k band is reduced, then the interaction is stronger and a considerable depletion of the energy levels in the largest scales arises. This is in agreement with the large-scale forced

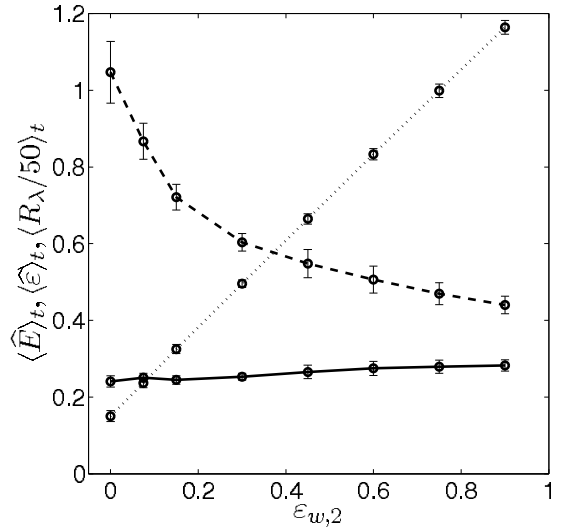


FIG. 5: Time-averaged total energy \widehat{E} (solid), total energy dissipation rate $\widehat{\varepsilon}$ (dotted) and Taylor-Reynolds number R_λ (dashed) for two-band forced turbulence with varying strength in the second band $\varepsilon_{w,2}$ at $Re = 1061$.

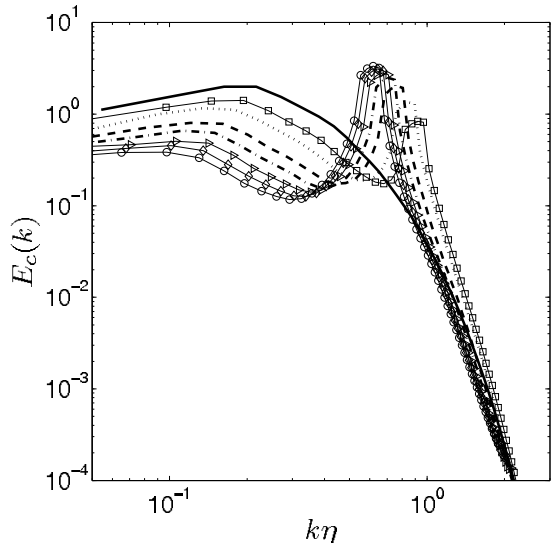


FIG. 6: Compensated shell- and time-averaged energy spectrum $E_c(k)$ for forced turbulence in the band $\mathbb{K}_{17,20}$ at different strengths of forcing $\varepsilon_{w,2}$ and $Re = 1061$. Large-scale forcing only (solid), additional second band forcing with $\varepsilon_{w,2} = 0.07, 0.15, 0.30, 0.45, 0.60, 0.75, 0.90$ denoted as $\square, \square, \square, \square, \square, \triangleright, \diamond, \circ$, respectively. In each case $\varepsilon_{w,1} = 0.15$.

turbulence results, where the local and non-local interactions were found to be energetically dominant while the distant interactions were mainly responsible for transferring structural information [29].

An effective modulation of turbulent quantities is possible not only by a change in the range of forced modes

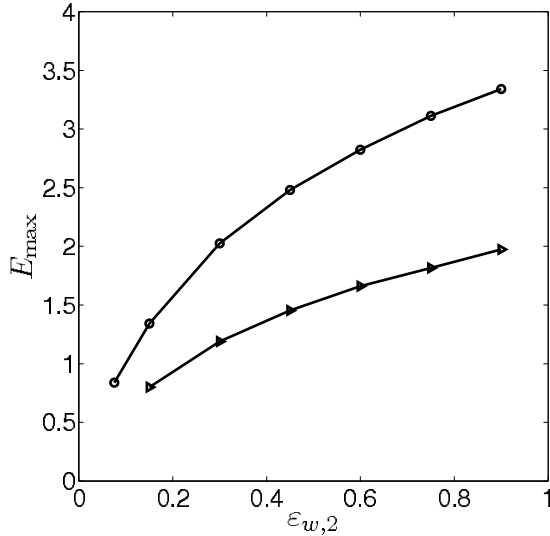


FIG. 7: Value of the maximum energy $E_{\max} = \max_k (E_c(k))$ in the forced region for four-shell $\mathbb{K}_{17,20}$ (\circ) and eight-shell $\mathbb{K}_{17,24}$ (\triangleright) forced turbulence, measured from the compensated spectra at $Re = 1061$.

but also via a change in the energy input rate. To investigate this we adopted an energy injection rate $\varepsilon_{w,1} = 0.15$ for the large-scale forcing in \mathbb{S}_1 and we vary the intensity of forcing in the second band by changing $\varepsilon_{w,2}$. We adopted the following values for $\varepsilon_{w,2}$: 0.07, 0.15, 0.30, 0.45, 0.60, 0.75 or 0.90 and considered forcing of four or eight shells in $\mathbb{K}_{17,20}$ or $\mathbb{K}_{17,24}$, respectively. The parameters and characteristic quantities can be found in Table I and II as Runs 2 – 7 and 8 – 13.

The total energy in the system is only slightly affected by the forcing-strength in the second band as shown in Fig 5. An increased forcing strength introduces additional energy into the flow at small scales that is dissipated very efficiently. This is expressed by the linear increase in $\langle \varepsilon \rangle_t$. In Fig. 6 we present the compensated energy spectrum for various strengths of the forcing $\varepsilon_{w,2}$. The energy in the forced region reaches higher values with increasing $\varepsilon_{w,2}$. This may be further observed in terms of the energy maximum $E_{\max} = \max_k (E_c(k))$ in Fig. 7. Changing the strength of the broad-band forcing induces a characteristic depletion in the larger scales. This suggests that the additional forcing term enhances the nonlinear interactions, which influence various scales quite far away from the forced region. The energy that is injected at the larger scales is transferred even more effectively through the cascade as $\varepsilon_{w,2}$ increases. This effect appears similar to the so-called spectral short-cut observed in nature and experiments [25]. In case of such a short-cut the energy from larger scales is diverted quite directly to fine scales largely by-passing the traditional cascading. This mechanism was explained in the case of flow over forest-canopies in [25]. We will investigate it in more detail in the next section.

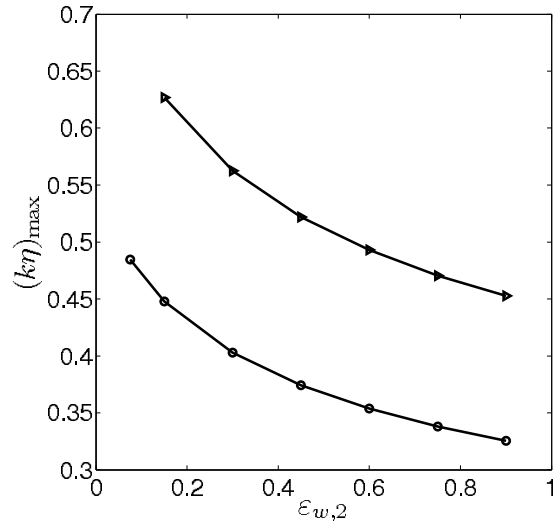


FIG. 8: Location of the maximum energy in the forced region for four-shell $\mathbb{K}_{17,20}$ (\circ) and eight-shell $\mathbb{K}_{17,24}$ (\triangleright) forced turbulence, measured from the compensated spectra at $Re = 1061$.

While the energy-maximum E_{\max} shifts to higher values with increasing strength of the high- k forcing, the location of the peak moves towards larger scales. This may be seen from the value of $(k\eta)_{\max}$ at which the maximum of $E_c(k)$ is attained (cf. Fig. 8). If we inject the same amount of energy to $\mathbb{K}_{17,24}$ that is two times wider than $\mathbb{K}_{17,20}$ the maximum of the response decreases (cf. Fig. 7) while the location of the peak moves towards smaller scales (cf. Fig. 8). These numerical experiments are in agreement with observations for decaying turbulence in which initially additional energy is assigned to small scales [32]. The non-local energy cascade toward the small scales was found to increase remarkably during the initial period of decay. This is quite similar to our observed increase of the dissipation rate arising from an increased forcing of the high- k band.

A final quantification of the non-local effect on the spectrum that arises from the high- k forcing is collected in Fig. 9. Here we displayed the normalized accumulated energy

$$S_E(k) = \frac{\sum_{k' \leq k} E_c(k')}{\sum_k E_c(k)} \quad (24)$$

in the consecutive shells. As pointed out, varying the properties of a flow in a specified spectral region can change the behavior of a flow well outside this region. In terms of $S_E(k)$ we notice that close to 90% of the energy is present in the first 10 shells (Fig. 9) when only the large-scale forcing is applied. Influencing the flow at smaller scales in $\mathbb{K}_{17,20}$ is seen to remove most of the energy from these larger scales while there is only a slight impact on the dynamics of small scales. This effect becomes more pronounced with increasing $\varepsilon_{w,2}$. The underlying changes in the energy transfer will be considered in more detail in Sec. IV.

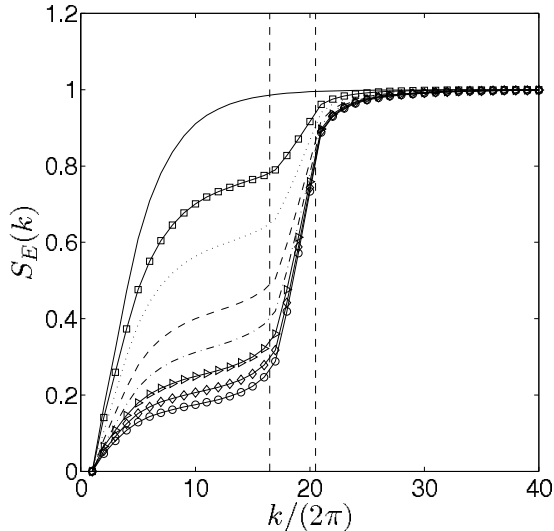


FIG. 9: Normalized accumulated energy $S_E(k)$ for two-band \mathbb{S}_1 and $\mathbb{K}_{17,20}$ forced turbulence at $Re = 1061$. Large-scale forcing at $\varepsilon_{w,1} = 0.15$ (solid) with additional second band forcing at $\varepsilon_{w,2} = 0.07, 0.15, 0.30, 0.45, 0.60, 0.75, 0.90$ is denoted by the \square , dotted, dashed, dash-dotted, \triangleright , \diamond and \circ curves, respectively.

B. Energy transfer spectra

The transfer of energy in turbulence can be described in spectral space as interactions of triads of wavevectors $(\mathbf{k}, \mathbf{p}, \mathbf{q})$ that form triangles, i.e., $\mathbf{k} = \mathbf{p} + \mathbf{q}$. Direct numerical simulation with large-scale forcing shows that non-local interactions between wavevectors combine into a local energy flow [13, 30]. By applying forcing that is located in a high- k range of spectral space we perturb the ‘natural’ cascading process. The associated changes in the transfer of energy will be investigated in more detail in this subsection. Specifically, we focus on the energy transfer and energy transport power spectra.

In large-scale forced turbulence energy is injected into the first shell and removed by the transfer term. This gives rise to negative values for the energy transfer in the forced region. In the higher shells the transfer function takes on positive values which illustrates the transfer of energy through the cascade toward higher k . By invoking the broad-band forcing we influence this basic energy cascade. This is clearly seen in the energy transfer spectrum which develops distinctive regions where $T(k) = \langle T(k, t) \rangle_t$ is negative. In Fig. 10 the effect of variations in the spectral support of the forcing is shown while Fig. 11 characterizes changes in the transfer function due to an increased forcing strength of the high- k band. The transfer function reaches lower values between the low- and high- k forcing regions compared to the large-scale forced case. The reverse situation appears near the high- k forced band where the transfer increases with an increase of the forcing intensity. This is in agreement

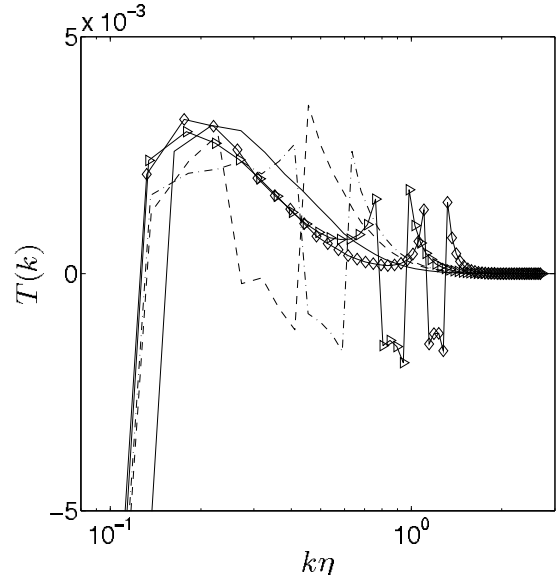


FIG. 10: Time-averaged energy transfer $T(k)$ for two-band forced turbulence. Large-scale forcing \mathbb{S}_1 (solid) with additional forcing in the $\mathbb{K}_{5,8}$ (dashed), $\mathbb{K}_{9,12}$ (dash-dotted), $\mathbb{K}_{17,20}$ (\triangleright), $\mathbb{K}_{25,28}$ (\diamond) band at $Re = 1061$.

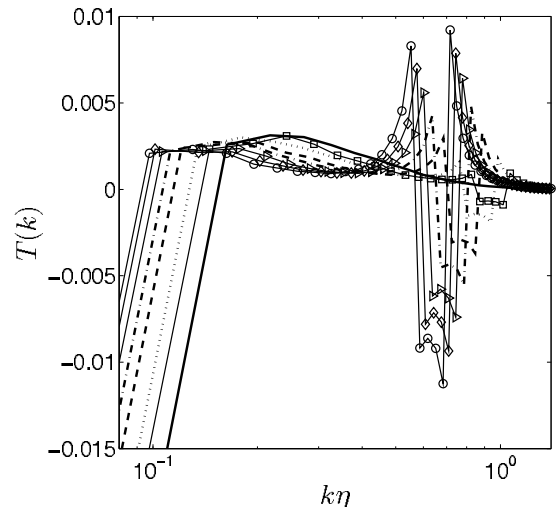


FIG. 11: Time-averaged energy transfer $T(k)$ for two-band \mathbb{S}_1 and $\mathbb{K}_{17,20}$ forced turbulence for different strengths of forcing in the second band $\varepsilon_{w,2}$ at $Re = 1061$. Large-scale forcing (solid) with additional second band forcing at $\varepsilon_{w,2} = 0.07, 0.15, 0.30, 0.45, 0.60, 0.75, 0.90$ denoted by \square , dotted, dashed, dash-dotted, \triangleright , \diamond and \circ curves, respectively.

with the energy spectra presented earlier, where we observed the depletion of energy between the forced regions. This effect can be observed more directly from spectra of energy transport power that will be presented next.

The energy transport power gives the rate at which energy is transferred from shells $k' < k$ to those with $k' > k$:

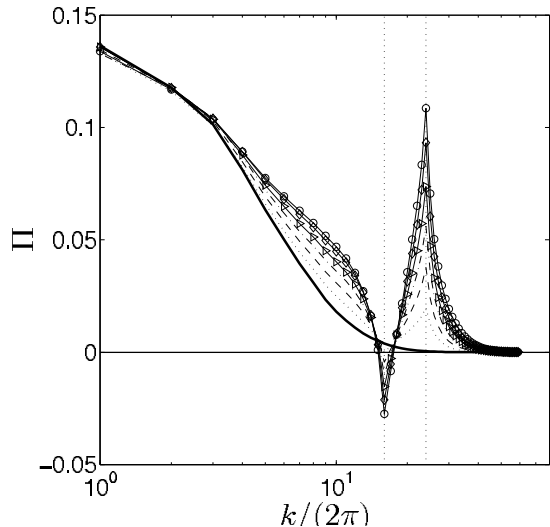


FIG. 12: Time-averaged transport power spectra for broadband forced turbulence in the $\mathbb{K}_{17,24}$ band at $Re = 1061$. Large-scale forcing (solid) with additional second band forced at $\varepsilon_{w,2} = 0.15, 0.30, 0.45, 0.60, 0.75, 0.90$ denoted as dotted, dashed, dash-dotted, \triangleright , \diamond , \circ curves, respectively. The supplementary forced region $k_1 < k \leq k_2$ is denoted with dotted lines.

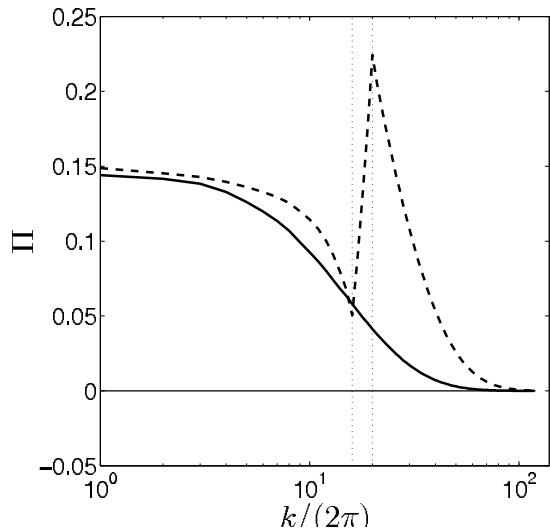


FIG. 13: Time-averaged transport power spectra for Reynolds number $Re = 4243$ and forcing in the $\mathbb{K}_{17,20}$ band. Large-scale forcing (solid), additional broadband forcing in the $\mathbb{K}_{17,20}$ band with $\varepsilon_{w,2} = 0.30$ (dashed).

$$\Pi(k, t) = \int_k^{k_{\max}} T(k', t) dk' = - \int_0^k T(k', t) dk', \quad (25)$$

where $k_{\max} = \pi N/L_b$ is the cut-off wavenumber. We present the time-averaged transport power spectrum

$\Pi(k) = \langle \Pi(k, t) \rangle_t$ in Fig. 12 for forcing with various strengths in the $\mathbb{K}_{17,24}$ band. In case of large-scale forcing only, the transport power is positive for all k as the energy is transferred toward smaller scales and reaches zero for large k indicating the general property of the total transfer function $\widehat{T}(t) = 0$. The application of high- k forcing for $k_1 < k \leq k_2$ changes this well-known picture. First, we note that the values of the transport power are all similar in the largest scales, where the flow is governed by the same energy input. The transport power for $0 < k \leq k_1$ becomes larger at higher $\varepsilon_{w,2}$. A striking change of the behavior arises for k near and inside the high- k forced region. The transport power spectrum even assumes negative values for $k \approx k_1$.

The observed behavior of the transport power in Fig. 12 is partly due to the relatively low Reynolds number that was used. At sufficiently high Reynolds numbers, the dissipation scales are much more separated from the high- k forced scales. In this case a plateau of Π will arise at low wavenumbers: $\Pi(k, t) \approx \varepsilon_{w,1}$ for k low enough [1]. This property is not observed at the computational Reynolds number considered so far.

In cases specified by Runs 18 – 19 we consider the flow at a four times higher computational Reynolds number. The overall results for the energy spectra and energy transfer were found to be qualitatively the same as in the lower Reynolds number cases. However, a plateau may now be observed in Fig. 13, where we present the transport power for the higher Reynolds number. In this case the transport power does not decrease below zero in the forced region. The second forcing band is well separated from the dissipation region and the transport power in this band is much larger, approaching a maximum 0.23 that is near the energy injection rate $\varepsilon_{w,2}$.

In this section we have looked at the effect of high- k modulation of the energy cascading process that leads to an increased energy dissipation in small scales. This process is supported by an increased energy transfer to smaller scales via nonlocal triad interactions. The effect of increased energy rate by the application of broadband forcing is seen in the energy transfer and transport power spectra. In the next section we will look more closely at the interactions of various scales of motion under the influence of broadband forcing by considering the two- and three-mode transfers T_p and T_{pq} introduced in (22) and (20).

IV. TWO- AND THREE-MODE INTERACTION OF SCALES

The energy dynamics of turbulent flow is generally discussed in terms of the transfer of kinetic energy from larger to smaller scales through nonlinear interactions. The statistical properties of turbulence are determined by these interactions. In the previous section we have shown how additional broadband forcing of inertial range scales can modify the classical picture of the Kolmogorov cas-

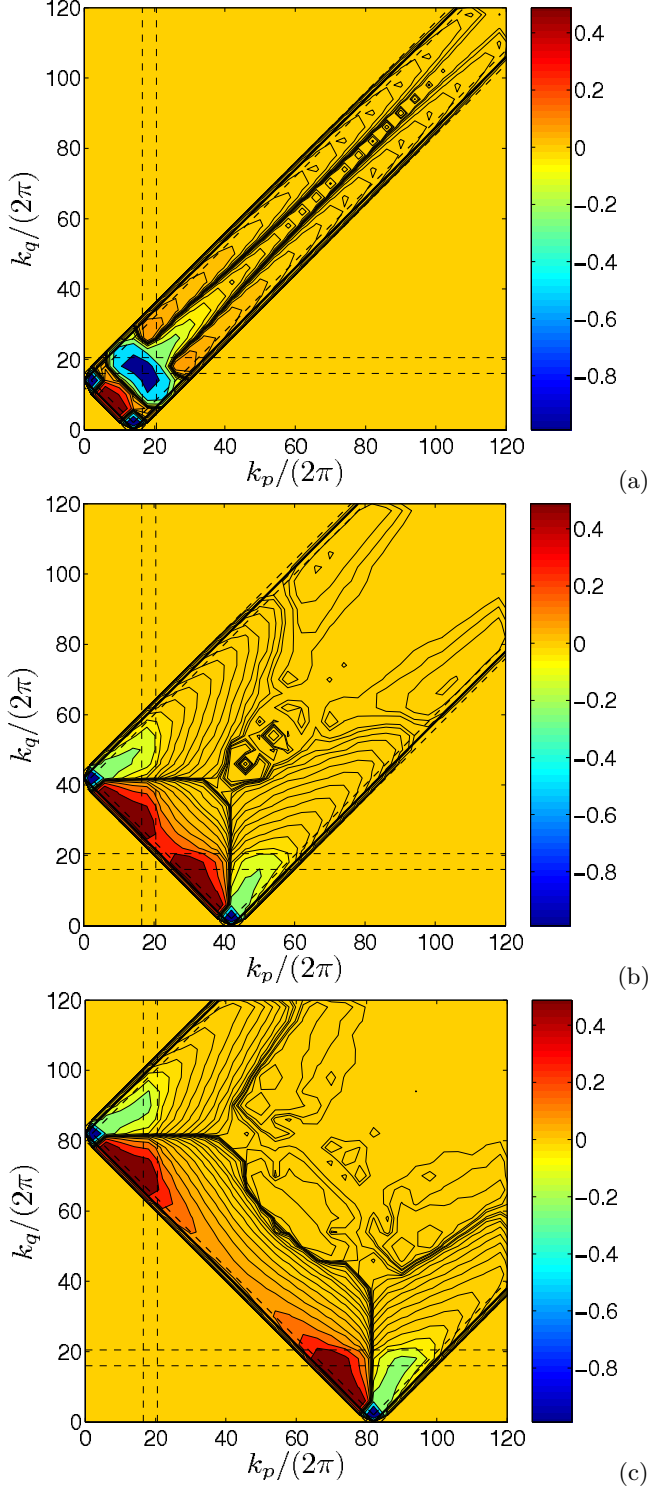


FIG. 14: The normalized triad energy transfer function $\overline{T}_{pq}(k, k_p, k_q)$ for $k/(2\pi) = 14, 42, 82$ in (a), (b), (c), respectively. The dashed lines correspond to the lower (k_1) and upper (k_2) wavenumbers used in the broad-band forcing at $Re = 4243$. The contour levels are $\pm 1/2^n$, $n = 0, \dots, 18$ that are the same for all three pictures.

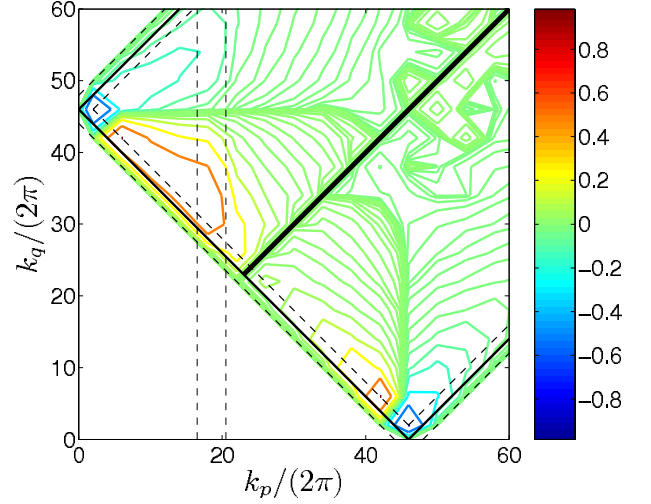


FIG. 15: The normalized triad energy transfer function $\overline{T}_{pq}(k, k_p, k_q)$ for $k/(2\pi) = 46$ at $Re = 4243$. The upper (bottom) rectangle presents broad-band (large-scale) forced turbulence respectively. The contour levels are $\pm 1/2^n$, $n = 0, \dots, 24$.

cade. To investigate the observed turbulence modulation effects in more detail we consider the underlying two- and three-mode energy transfer terms in this section. This will clarify to some extent the changes in the various nonlinear interactions that give rise to the observed alterations in the spectra and energy transfer.

We start with the three-mode transfer that is averaged in time $T_{pq}(k, k_p, k_q) = \langle T_{pq}(k, k_p, k_q, t) \rangle_t$ and split this term into its positive and negative parts:

$$T_{pq}(k, k_p, k_q) = T_{pq}^-(k, k_p, k_q) + T_{pq}^+(k, k_p, k_q), \quad (26)$$

in which

$$T_{pq}^+(k, k_p, k_q) = \begin{cases} T_{pq}(k, k_p, k_q) & \text{if } T_{pq}(k, k_p, k_q) \geq 0, \\ 0 & \text{otherwise,} \end{cases} \quad (27)$$

with a similar definition for the negative part:

$$T_{pq}^-(k, k_p, k_q) = \begin{cases} T_{pq}(k, k_p, k_q) & \text{if } T_{pq}(k, k_p, k_q) < 0, \\ 0 & \text{otherwise.} \end{cases} \quad (28)$$

In terms of these contributions we examine the normalized triad energy transfer

$$\overline{T}_{pq}(k, k_p, k_q) = \frac{T_{pq}^-(k, k_p, k_q)}{T_{\min}(k)} + \frac{T_{pq}^+(k, k_p, k_q)}{T_{\max}(k)}, \quad (29)$$

where

$$\begin{aligned} T_{\min}(k) &= -\min_{k_p, k_q} (T_{pq}^-(k, k_p, k_q)), \\ T_{\max}(k) &= \max_{k_p, k_q} (T_{pq}^+(k, k_p, k_q)). \end{aligned} \quad (30)$$

Through the scaling of T_{pq}^- and T_{pq}^+ with T_{\min} and T_{\max} respectively, the normalized transfer is well suited

to characterize the overall structure of the three-mode transfer function, even in cases in which the order of magnitude of T_{pq} varies considerably. The normalized energy transfer $\bar{T}_{pq}(k, k_p, k_q)$ is plotted in Fig. 14 for three different wavenumbers $k/(2\pi) = 14, 42, 82$, based on Run 19 in which $R_\lambda \cong 75$. The three k -values that are selected correspond to wavenumbers below the forced region ($k/(2\pi) = 14$) or to wavenumbers that are considerably larger. Such contour maps for \bar{T}_{pq} can also be found in [19] for the case of large-scale forced turbulence. For completeness, we also presented the results from such large-scale forced turbulence (Run 18) comparing these directly to the broad-band forced turbulence (Run 19). This contour map is shown in Fig. 15 for $k/(2\pi) = 46$.

The strongest interactions are observed for modes with wavenumbers between the largest forced scales and the high- k forced region as can be seen in Fig. 14(a). As in the case of large-scale forcing only we observe very strong interactions between Fourier modes of considerably different scales. These are located in the corners of the rectangular domains in the k_p - k_q plane. Distant interactions are well separated from the origin in these figures. Their contribution to the transfer is seen to be very small, as also noticed earlier in the literature [19]. The change of sign in the transfer function that occurs at $k_p = k$ and $k_q = k$ respectively on the k_p - k_q planes indicates that in this region the energy is mainly transferred to higher k .

The most efficient transfer takes place between two wavevectors of similar size and one of quite different size as seen in the corners of the rectangular area in Fig. 14. This is in agreement with previous numerical experiments reported by various authors [2, 16, 19]. However, compared to the case of large-scale forcing only, we now observe quite extended, highly energetic interactions with the high- k forced region. The second forced band causes regions with high intensity of interactions to be much wider compared to the case of large-scale forcing only. This is visible directly in Fig. 15. The regions with positive and negative transfer are extended from the corners to the wavenumber regions where the actual application of forcing in the second band occurs. The energy is exchanged predominantly between scales that are more separated than in case of the large-scale forced flow where the dominant interactions occur only in the corners. This is a clear indication of the stronger non-local interactions, mentioned earlier.

For further clarification of energy transfer processes we turn to the time-averaged two-mode energy transfer $T_p(k, k_p) = \langle T_p(k, k_p) \rangle_t$, which gives information about the interactions involving a sum over all k_q wavenumbers at fixed k and k_p . The sum involves all k_q wavenumbers that are constrained by the triadic interactions, i.e., their length may vary between $|\mathbf{k} - \mathbf{p}|$ and $|\mathbf{k} + \mathbf{p}|$. We normalized the two-mode transfer function $T_p(k, k_p)$ in a similar

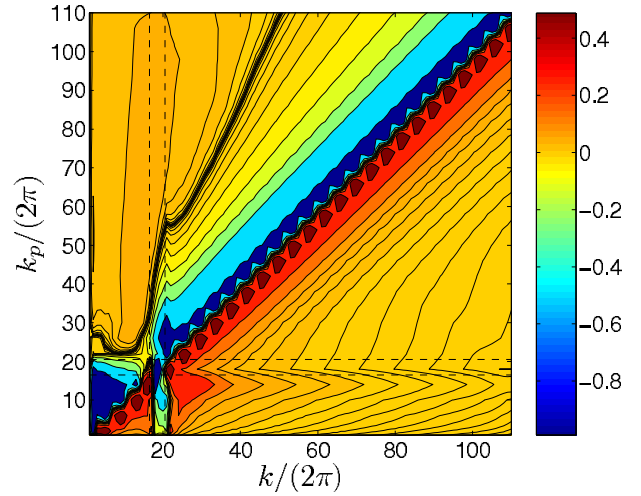


FIG. 16: The normalized triad energy transfer function $\bar{T}_p(k, k_p)$ at $Re = 4243$ (Run 19). The contour levels are $\pm 1/2^n$, $n = 0, \dots, 18$. The supplementary forced region $k_1 < k \leq k_2$ denoted with dashed lines.

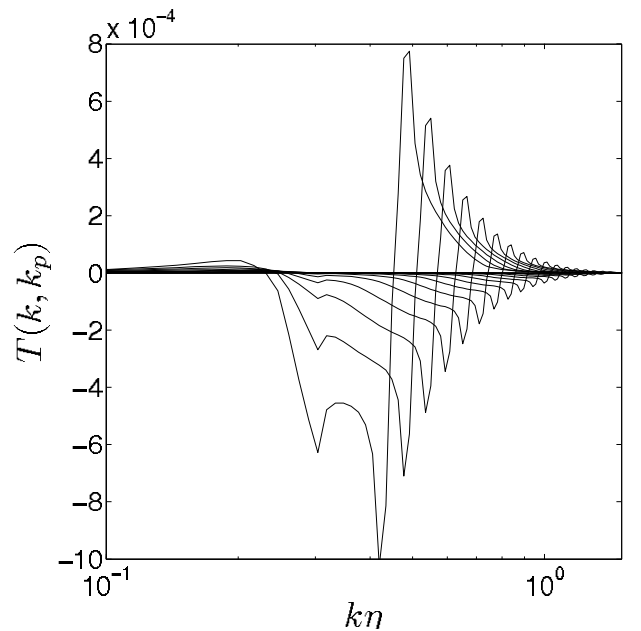


FIG. 17: The triad energy transfer function $T_p(k, k_p)$ at $k_p/(2\pi) = 30, 34, \dots, 94$ and $Re = 4243$ (Run 19).

manner as $T_p(k, k_p, k_q)$:

$$\bar{T}_p(k, k_p) = \frac{T_p^-(k, k_p)}{T_{\min}(k)} + \frac{T_p^+(k, k_p)}{T_{\max}(k)}, \quad (31)$$

where T_p^\pm , T_{\min} and T_{\max} are defined in terms of T_p in a manner analogous to the definitions in (26), (27), (28) and (30). In Fig. 16 we plotted the contour map of $\bar{T}_p(k, k_p)$. For larger wavenumbers this quantity was found to look quite similar to the case of large-scale forced

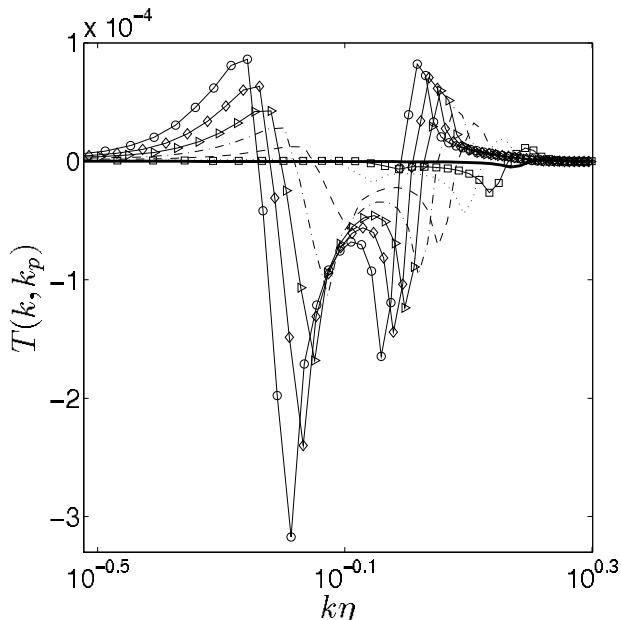


FIG. 18: The triad energy transfer function $T_p(k, k_p)$ at $k_p/(2\pi) = 30$ and $Re = 1061$. Large-scale forcing (solid) with additional second band forced at $\varepsilon_{w,2} = 0.07, 0.15, 0.30, 0.45, 0.60, 0.75, 0.90$ denoted as \square , dotted, dashed, dash-dotted, \triangleright , \diamond , \circ , respectively.

turbulence. The two-mode transfer function changes sign from negative to positive at $k = k_p$ indicating a downward energy flow. Comparing this to the large-scale forced turbulence we observe (i) strong influence of forcing in the regions where it is applied (denoted with dashed lines), (ii) extended negative energy transfer region with comparatively high magnitude above the $k = k_p$ line, (iii) amplification of the backward energy transfer indicated by the positive region for small k and large k_p . This region is separated from the intense negative energy transfer region by the indicated accumulation of contour lines above the $k = k_p$ line appearing as the curved black line.

A more quantitative overview is plotted in Fig. 17 displaying the two-mode transfer function in the range $k_p/(2\pi) = 30, 34, \dots, 94$. This clearly shows the cascading character of the energy flow from larger to smaller scales in the system. The modification due to the high- k forcing expresses itself by the sequence of one slightly positive, two quite negative and one quite positive local extrema. The intensity of the energy transfer decreases with increasing wavenumbers as less energy needs to be transferred. This corresponds directly to the magnitude of $T_{\min}(k)$ and $T_{\max}(k)$ used in the normalization of $T_p(k, k_p)$ (31). The part in which the transfer is negative is much wider in the broad-band forced case compared to the large-scale forced turbulence results.

We conclude by considering the effect of varying the forcing strength $\varepsilon_{w,2}$ at a characteristic wavenumber $k_p/(2\pi) = 30$ on the two-mode energy transfer function

$T_p(k, k_p)$. This is shown in Fig. 18. In the large-scale forced case at $\varepsilon_{w,2} = 0$ the transfer is very small compared to the cases in which the high- k forcing is active. In addition, the effect is very localized (solid line in Fig. 18). The forcing in the high- k band completely changes this behavior. The intensity of the energy transfer is directly related to the value of $\varepsilon_{w,2}$. Additional extrema appear in the two-mode transfer function. The high- k forced cases display two pairs in which a negative minimum is combined with a positive maximum, while large scale forcing only yields one such combination. Correspondingly, the min-max pair at high k is associated with the large scale forcing in S_1 while the min-max pair at lower k originates from the additional forcing in the second band. We also investigated three-band forcing and observed further peaks in the energy transfer spectra.

V. CONCLUDING REMARKS

We performed direct numerical simulations of broad-band forced turbulence to explore accumulated effects on the time-averaged energy transfer in isotropic homogeneous turbulence. Using broad-band forcing based on a recently proposed mathematical model for a fractal stirrer [27] we have shown how the application of such forcing modulates turbulence both qualitatively and quantitatively. The modulation is similar to that observed in experiments based on flows through porous media or canopies. Specifically the perturbation of a flow arising from the contact with complex physical boundaries enhances the dissipation and causes an abrupt energy drain from large to small scales. This aspect of simultaneous perturbation of a flow on a spectrum of length-scales is retained in the cases studied here.

We found that broad-band forcing that perturbs a turbulent flow at smaller scales enhances non-local triad interactions and alters the detailed cancellation processes that occur in the traditional large-scale forced flows. This leads to non-local modifications in the energy transfer spectrum and the energy distribution among scales. We verified this by partitioning the nonlinear term in the Navier–Stokes equations in terms of different triad contributions to the total transfer function. The energy transport power is found to be enhanced in the spectral region in between the large-scale and the high- k forced bands. This characteristic may be influenced via the control parameters of the applied forcing, i.e., its strength and extent of agitated scales, and allows optimizing transport processes of turbulent flows.

Future study will involve the examination of the consequences of forcing in the physical space context. We will investigate the geometrical statistics of broad-band forced turbulence looking at the interactions of strain and vorticity and their modulation by the applied forcing. This may help understanding which physical processes are responsible for the observed modulations and how to exploit this to enhance physical space mixing.

| Run | ε_w | m | p | Run | ε_w | m | p |
|-----|-----------------|-----|-----|-----|-----------------|-----|-----|
| 1 | 0.15* | — | — | | | | |
| 2 | 0.07 | 17 | 20 | 8 | 0.15 | 17 | 24 |
| 3 | 0.30 | 17 | 20 | 9 | 0.30 | 17 | 24 |
| 4 | 0.45 | 17 | 20 | 10 | 0.45 | 17 | 24 |
| 5 | 0.60 | 17 | 20 | 11 | 0.60 | 17 | 24 |
| 6 | 0.75 | 17 | 20 | 12 | 0.75 | 17 | 24 |
| 7 | 0.90 | 17 | 20 | 13 | 0.90 | 17 | 24 |
| 14 | 0.15 | 5 | 8 | 18 | 0.15* | — | — |
| 15 | 0.15 | 9 | 12 | 19 | 0.30 | 17 | 20 |
| 16 | 0.15 | 17 | 20 | | | | |
| 17 | 0.15 | 25 | 28 | | | | |

TABLE I: Direct numerical simulation parameters using a resolution of $N = 128$ and $Re = 1061$ in Runs 1 – 17, and a resolution of $N = 256$ at $Re = 4243$ in Runs 18 – 19. The cases with large-scale forcing only are denoted by \star . In this table ε_w denotes the energy input-rate in the high- k band, except Run 1 and 18 in which it corresponds to the energy input-rate in S_1 . Moreover, m and p characterize the spectral support of the high- k band $\mathbb{K}_{m,p}$.

APPENDIX

The main parameters of the simulations are collected in Table I. The corresponding statistics of the velocity fields are summarized in Table II. The quantities compiled in Table II are the Kolmogorov dissipation wavenumber k_d which is the inverse of the Kolmogorov length-scale η , the product $k_{\max}\eta$, the Taylor microscale $\lambda = (5\widehat{E}/\sum_{\mathbf{k}} k^2 E(\mathbf{k}, t))^{1/2}$, the Taylor-microscale Reynolds number $R_\lambda = \lambda u'/\nu$, the integral length-scale $L = 3\pi/(4\widehat{E})\sum_{\mathbf{k}} k^{-1} E(\mathbf{k}, t)$, the integral Reynolds number $R_L = Lu'/\nu$, the r.m.s velocity $u' = (2\widehat{E}/3)^{1/2}$, the energy dissipation rate $\varepsilon = \sum_{\mathbf{k}} 2\nu k^2 E(\mathbf{k}, t)$, the eddy-turnover time $\tau = L/u'$ and the skewness $S = 2/35(\lambda/u')^3 \sum_{\mathbf{k}} k^2 T(\mathbf{k}, t)$. All these quantities in Table II are time-averaged $\langle \cdot \rangle_t$ as described in Sec. IID.

We also checked that the alteration of the cascading process caused by the high- k forcing does not influence the isotropy of the flow field. A measure of isotropy was suggested in [38] given by: $I^2(t) = \psi_1(t)/\psi_2(t)$ where $\psi_1(t) = \langle |\mathbf{e}_1(\mathbf{k})\mathbf{u}(\mathbf{k}, t)|^2 \rangle$, $\psi_2(k, t) = \langle |\mathbf{e}_2(\mathbf{k})\mathbf{u}(\mathbf{k}, t)|^2 \rangle$ are

the kinetic energy along the components of two orthogonal solenoidal unit vectors $\mathbf{e}_1(\mathbf{k}) = \mathbf{k} \times \mathbf{z}(\mathbf{k})/|\mathbf{k} \times \mathbf{z}(\mathbf{k})|$, $\mathbf{e}_2(\mathbf{k}) = \mathbf{k} \times \mathbf{e}_1(\mathbf{k})/|\mathbf{k} \times \mathbf{e}_1(\mathbf{k})|$ where $\mathbf{z}(\mathbf{k})$ is a randomly oriented unit vector. The operator $\langle \cdot \rangle$ denotes averaging over these random unit vectors. For isotropic turbulence one can expect to find $I = 1$, i.e., $\psi_1 = \psi_2$ which was confirmed to close approximation in all simulations. Deviations from the expected value for I were found to be of the order of 1%.

| Run | k_d | $k_{\max}\eta$ | λ | R_λ | L | R_L | u' | ε | τ | S |
|-----|-------|----------------|-----------|-------------|------|-------|------|---------------|--------|------|
| 1 | 116 | 3.26 | 0.123 | 52 | 0.23 | 97 | 0.40 | 0.15 | 0.57 | 0.49 |
| 2 | 130 | 2.91 | 0.100 | 43 | 0.23 | 100 | 0.41 | 0.24 | 0.56 | 0.35 |
| 3 | 156 | 2.42 | 0.069 | 30 | 0.23 | 98 | 0.41 | 0.50 | 0.54 | 0.21 |
| 4 | 168 | 2.25 | 0.061 | 27 | 0.23 | 101 | 0.42 | 0.66 | 0.54 | 0.17 |
| 5 | 178 | 2.12 | 0.056 | 25 | 0.22 | 102 | 0.43 | 0.83 | 0.52 | 0.15 |
| 6 | 186 | 2.03 | 0.051 | 23 | 0.22 | 102 | 0.43 | 1.00 | 0.52 | 0.14 |
| 7 | 193 | 1.95 | 0.048 | 22 | 0.22 | 100 | 0.43 | 1.16 | 0.50 | 0.13 |
| 8 | 140 | 2.68 | 0.085 | 37 | 0.23 | 99 | 0.41 | 0.33 | 0.56 | 0.29 |
| 9 | 156 | 2.41 | 0.070 | 31 | 0.23 | 102 | 0.41 | 0.50 | 0.56 | 0.22 |
| 10 | 169 | 2.24 | 0.060 | 26 | 0.22 | 98 | 0.41 | 0.68 | 0.54 | 0.18 |
| 11 | 178 | 2.11 | 0.054 | 24 | 0.22 | 100 | 0.42 | 0.85 | 0.53 | 0.16 |
| 12 | 187 | 2.02 | 0.049 | 22 | 0.22 | 97 | 0.42 | 1.03 | 0.52 | 0.15 |
| 13 | 194 | 1.94 | 0.046 | 21 | 0.21 | 96 | 0.42 | 1.20 | 0.50 | 0.13 |
| 14 | 138 | 2.73 | 0.090 | 39 | 0.22 | 96 | 0.41 | 0.30 | 0.52 | 0.44 |
| 15 | 138 | 2.72 | 0.089 | 39 | 0.23 | 102 | 0.42 | 0.31 | 0.56 | 0.39 |
| 16 | 140 | 2.69 | 0.084 | 36 | 0.22 | 96 | 0.40 | 0.33 | 0.55 | 0.28 |
| 17 | 143 | 2.64 | 0.082 | 36 | 0.23 | 98 | 0.41 | 0.35 | 0.56 | 0.22 |
| 18 | 325 | 2.32 | 0.065 | 115 | 0.21 | 368 | 0.42 | 0.15 | 0.50 | 0.51 |
| 19 | 432 | 1.74 | 0.040 | 75 | 0.21 | 394 | 0.44 | 0.46 | 0.47 | 0.38 |

TABLE II: Direct numerical simulations statistics of the different cases studied.

ACKNOWLEDGMENTS

This work is part of the research program ‘‘Turbulence and its role in energy conversion processes’’ of the Foundation for Fundamental Research of Matter (FOM). The authors wish to thank NCF (Dutch foundation for National Computing Facilities) for supporting the computations. These were executed at SARA Computing and Networking Services in Amsterdam.

-
- [1] W. D. McComb. *The Physics of Fluid Turbulence*. Oxford University Press, 1990.
 - [2] Y. Zhou and Ch. G. Speziale. Advances in the fundamental aspects of turbulence: Energy transfer, interacting scales, and self-preservation in isotropic decay. *Appl. Mech. Rev.*, 51(4):267–301, 1998.
 - [3] E. D. Siggia. Numerical study of small-scale intermittency in three-dimensional turbulence. *J. Fluid Mech.*, 107:375–406, 1981.
 - [4] R. M. Kerr. Higher-order derivative correlations and the

- alignment of small-scale structures in isotropic numerical turbulence. *J. Fluid Mech.*, 153:31–58, 1985.
- [5] V. Eswaran and S. B. Pope. An examination of forcing in direct numerical simulations of turbulence. *Comput. Fluids*, 16:257–278, 1988.
- [6] S. Chen and X. Shan. High-resolution turbulent simulations using the Connection Machine-2. *Comput. Phys.*, 6(6):643–646, 1992.
- [7] J. Jimenez, A. A. Wray, P. G. Saffman, and R. S. Rogallo. The structure of intense vorticity in isotropic turbulence.

- J. Fluid Mech.*, 255:65–90, 1993.
- [8] S. Ghosal, T. S. Lund, P. Moin, and K. Akselvoll. A dynamic localization model for large-eddy simulation of turbulent flows. *J. Fluid Mech.*, 286:229–255, 1995.
- [9] L. Machiels. Predictability of small-scale motion in isotropic fluid turbulence. *Phys. Rev. Lett.*, 79(18):3411–3414, 1997.
- [10] M. R. Overholt and S. B. Pope. A deterministic forcing scheme for direct numerical simulations of turbulence. *Comput. Fluids*, 27(1):11–28, 1998.
- [11] Y. Kaneda, T. Ishihara, M. Yokokawa, K. Itakura, and A. Uno. Energy dissipation rate and energy spectrum in high resolution direct numerical simulations of turbulence in a periodic box. *Phys. Fluids*, 15(2):L21–L24, 2003.
- [12] A. N. Kolmogorov. The local structure of turbulence in incompressible viscous fluids at very large Reynolds numbers. *C.R. Acad. Sci. URSS*, 30:301–305, 1941.
- [13] Y. Zhou. Degrees of locality of energy transfer in the inertial range. *Phys. Fluids A*, 5(5):1092–1094, 1993.
- [14] J. A. Domaradzki, R. W. Metcalfe, R. S. Rogallo, and J. J. Riley. Analysis of subgrid-scale eddy viscosity with use of results from Direct Numerical Simulations. *Phys. Rev. Lett.*, 58(6):547–550, 1987.
- [15] J. A. Domaradzki. Analysis of energy transfer in direct numerical simulations of isotropic turbulence. *Phys. Fluids*, 31(10):2747–2749, 1988.
- [16] J. A. Domaradzki and R. S. Rogallo. Local energy transfer and nonlocal interactions in homogeneous, isotropic turbulence. *Phys. Fluids A*, 2(3):413–426, 1990.
- [17] J. A. Domaradzki. Nonlocal triad interactions and the dissipation range of isotropic turbulence. *Phys. Fluids A*, 4(9):2037–2045, 1992.
- [18] J. A. Domaradzki, W. Lui, C. Hartel, and L. Kleiser. Energy transfer in numerically simulated wall-bounded turbulent flows. *Phys. Fluids*, 6(4):1583–1599, 1994.
- [19] K. Ohkitani and S. Kida. Triad interactions in a forced turbulence. *Phys. Fluids A*, 4(4):794–802, 1992.
- [20] F. Waleffe. The nature of triad interactions in homogeneous turbulence. *Phys. Fluids A*, 4(2):350–363, 1992.
- [21] A. K. Kuczaj and B. J. Geurts. Mixing in manipulated turbulence. *J. Turbul.*, submitted.
- [22] W. D. McComb and K. T. J. Chan. Drag reduction in fibre suspension. *Nature*, 292:520–522, 1981.
- [23] W. D. McComb and K. T. J. Chan. Laser-Doppler anemometer measurements of the turbulent structure in drag-reducing fibre suspensions. *J. Fluid Mech.*, 152:455–478, 1985.
- [24] K. Boomsma, D. Poulikakos, and F. Zwick. Metal foams as compact high performance heat exchangers. *Mech. Mater.*, 35:1161–1176, 2003.
- [25] J. Finnigan. Turbulence in plant canopies. *Ann. Rev. Fluid Mech.*, 32:519–571, 2000.
- [26] A. Pouquet, U. Frisch, and J. P. Chollet. Turbulence with a spectral gap. *Phys. Fluids*, 26(4):877–880, 1983.
- [27] B. Mazzi and J. C. Vassilicos. Fractal generated turbulence. *J. Fluid Mech.*, 502:65–87, 2004.
- [28] P. K. Yeung and J. G. Brasseur. The response of isotropic turbulence to isotropic and anisotropic forcing at the large scales. *Phys. Fluids A*, 3(5):884–897, 1991.
- [29] J. G. Brasseur and Ch-H. Wei. Interscale dynamics and local isotropy in high Reynolds number turbulence within triadic interactions. *Phys. Fluids*, 6(6):842–870, 1994.
- [30] Y. Zhou. Interacting scales and energy transfer in isotropic turbulence. *Phys. Fluids A*, 5(10):2511–2524, 1993.
- [31] Y. Zhou, P. K. Yeung, and J. G. Brasseur. Scale disparity and spectral transfer in anisotropic numerical turbulence. *Phys. Rev. E*, 53(1):1261–1264, 1996.
- [32] Y. Suzuki and Y. Nagano. Modification of turbulent helical/nonhelical flows with small-scale energy input. *Phys. Fluids*, 11(11):3499–3511, 1999.
- [33] P. Moin and T. Bewley. Feedback control of turbulence. *Appl. Mech. Rev.*, 47:S3, 1994.
- [34] B. J. Geurts. *Elements of Direct and Large-Eddy Simulation*. R.T. Edwards, 2004.
- [35] C. Canuto, M. Hussaini, A. Quarteroni, and T. Zang. *Spectral Methods in Fluid Dynamics*. Springer Verlag (Berlin and New York), 1988.
- [36] P. K. Yeung, J. G. Brasseur, and Q. Wang. Dynamics of direct large-small scale couplings in coherently forced turbulence: concurrent physical- and fourier-space views. *J. Fluid Mech.*, 283:43–95, 1995.
- [37] W. D. McComb, A. Hunter, and C. Johnston. Conditional mode-elimination and the subgrid-modeling problem for isotropic turbulence. *Phys. Fluids*, 13(7):2030–2044, 2001.
- [38] J. H. Curry, J. R. Herring, J. Loncaric, and S. A. Orszag. Order and disorder in two- and three dimensional Bénard convection. *J. Fluid Mech.*, 147:1–38, 1984.